Engineering Structures 365 (2026) 123247

Contents lists available at ScienceDirect

Engineering Structures

journal homepage: www.elsevier.com/locate/engstruct

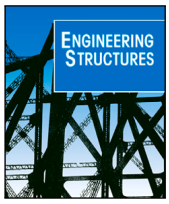

Timber connections with increased friction in the shear plane: Experimental and analytical investigations into strength and stiffness

Simon Aurand *, Hans Joachim Blass

KIT Timber Structures and Building Construction, Karlsruhe Institute of Technology (KIT), R.-Baumeister-Platz 1, Karlsruhe, 76131, Germany

ARTICLE INFO

Keywords:
Friction
Inclined screws
System connectors
Densified veneer wood
Timber connections
Analytical model
Stiffness

ABSTRACT

Timber connections with increased friction in the shear plane are studied, focusing on experimental and analytical approaches to enhance load-carrying capacity and stiffness. Conventional aluminium connectors, while structurally adequate, pose environmental and fire-resistance limitations. As an alternative, densified veneer wood (DVW) was introduced for system connectors, offering superior sustainability and fire performance. The research explores surface modifications to improve frictional behaviour, thereby optimizing strength and stiffness. Short-term push-out tests examined various surface treatments and screw configurations, revealing that pronounced surface structuring significantly increases ultimate load capacity, while flat, uniform surfaces better maintain stiffness. Long-term duration-of-load tests confirmed that frictional performance remains stable over time, with creep factors for inclined screws significantly lower than those for other dowel-type fasteners. An analytical model was developed to predict load-carrying capacity and stiffness, incorporating friction effects and deformation perpendicular to the grain. The mechanical model proposed in the new generation of EC5 overestimates the stiffness when used for connections with connector plates and inclined screws, because it neglects deformations perpendicular to the grain beneath the connector plate. In contrast, the herein presented spring model incorporates compression behaviour perpendicular to the grain, thus, predicting load-carrying capacity and stiffness accurately for a range of timber components, including CLT and GLT reinforced with fully threaded screws. The results demonstrate that DVW connectors with appropriately modified surfaces can achieve high ultimate loads and reliable long-term performance, thereby supporting their adoption in sustainable timber construction.

1. Introduction

1.1. Motivation and scope of paper

The design and performance of timber connections play a vital role in modern timber structures. Conventional joist-to-header connectors are widely available in various geometries, with dovetail-type interlocking systems being among the most common. These connectors are typically manufactured from aluminium, a material that, while offering adequate mechanical performance, presents limitations in terms of environmental impact and fire resistance. This study seeks to address these shortcomings by rethinking the concept of system connectors through the use of densified veneer wood (DVW) as an alternative material. DVW offers a significantly improved carbon footprint [1] and enhanced fire performance [2,3] compared to aluminium, aligning with the growing demand for sustainable and resilient building solutions.

Beyond material substitution, this research aims to increase the load-carrying capacity and stiffness of such connections. In traditional configurations, inclined screws transfer loads primarily through axial forces, generating compressive stresses perpendicular to the shear plane. These stresses create frictional resistance, which contributes to overall capacity. However, the magnitude of this contribution is strongly dependant on the coefficient of friction (COF) in the shear plane. To exploit this mechanism more effectively, the present work investigates surface modification strategies to enhance frictional behaviour within the shear plane, thereby improving both strength and stiffness.

The objective of this study was the development of analytical models capable of predicting key design parameters, specifically the characteristic load-carrying capacity $F_{2,\mathrm{Rk}}$ and the stiffness $K_{2,\mathrm{ser}}$. With such a model it is possible to integrate DVW-based connectors into engineering practice, providing reliable design equations that account for the combined effects of material properties, surface modifications, and connection geometry.

* Corresponding author.
E-mail address: aurand@kit.edu (S. Aurand).

https://doi.org/10.1016/j.engstruct.2026.123247
Received 18 February 2026; Received in revised form 15 May 2026; Accepted 17 June 2026
Available online 1 July 2026

Table 1
Material properties of DVW and GL 24h (COV in parenthesis).

Material properties	DVW			GL 24 h
	6 mm	10 mm	15 mm	
Density ρ_m [kg/m^3]	1363 (2%)	1376 (1%)	1381 (1%)	456[a] (5%)
Moisture content u [%]	7.1 (13%)	7.2 (16%)	6.7 (25%)	11.7[a] (7%)
Compression parallel to grain $f_{c,0,edge}$ [N/mm^2]	97.2 (9%)	96.9 (3%)	80.5 (10%)	24.0[b] (12%)[c]
Compression perp. to grain $f_{c,90,edge}$ [N/mm^2]	90.1 (4%)	88.9 (4%)	88.5 (4%)	2.5[b] (10%)[c]
MOE $E_{m,0,flat}$ [N/mm^2]	20300 (8%)	19500 (9%)	17600 (8%)	11500 (13%)[c]

[a] Determined herein.
[b] Characteristic strength acc. to EN 14080 [4].
[c] COV acc. to JCSS Probabilistic Model Code [5].

1.2. State of the art

In [6], it was shown that even a slight inclination of screws enables additional force transfer through friction between the connected components. As the inclination angle δ (i.e. angle between the fastener axis and the shear plane) decreases, the proportion of axial load in the total load-carrying capacity increases, while the contribution from lateral load diminishes. Due to the significant difference in stiffness between axial and lateral loading, almost the entire load is carried by axial forces, making the lateral component negligible.

Studies on steel-to-timber connections with inclined fully threaded screws were presented in [7], where an analytical model including friction was proposed for predicting total load-carrying capacity. A key aspect of this work was the effective number of fasteners n_{ef} in a group of axially loaded screws. The results suggest using $n_{ef} = 0.9 \cdot n$ for the ultimate limit state and $n_{ef} = n^{0.8}$ for the serviceability limit state.

In [8], the influence of friction on the load-carrying capacity of connections with dowel-type fasteners was investigated. Various surface modifications were considered; however, the friction studied was not in the shear plane between connected members but between timber and the fastener itself. Building on this, [9] conducted general tests to determine the friction coefficient of steel on wood. In [10], different surface modification processes aimed at increasing friction in the shear plane were examined, and friction coefficients were determined. The main findings were that all modifications increased friction in the shear plane and improved connection strength.

The stiffness of single-shear timber-to-timber connections has been investigated in several studies, e.g., [11,12]. These models are based on the lateral and axial slip modulus of screws and also consider friction in the shear plane. More recent studies on the analytical determination of the stiffness of steel-to-timber connections include [13–15]. All models rely on input parameters derived from test data, such as [16] for the axial stiffness of fully threaded screws. The main conclusion is that these models can predict the stiffness of timber-to-timber connections; however, they are limited to single-shear configurations and do not account for the stiffness of system connector plates.

The use of densified veneer wood (DVW) for system connectors is novel, although its application in timber structures dates back to at least the 1980s. In [17–19], DVW was investigated for use as dowel-type fasteners. In [2,3], the superior fire resistance of DVW compared to timber was demonstrated. The main findings were that DVW exhibits a lower charring rate than wood and lower heat transfer than steel, supporting the motivation for this study.

2. Materials and methods

2.1. Materials

For all tests glulam GL 24h (spruce/fir) was used. The wood was conditioned at 20 °C and 65% r.H. prior to the tests. The specimens were all cut from larger pieces from different manufacturers and batches. After the tests, the density and the moisture content were determined for all specimens on small-scale probes cut from the specimens close to the area of failure. The density of the wood varied between 380–530 kg/m^3 with a mean density of 456 kg/m^3 and a standard deviation of 25 kg/m^3. The results suggest that the density has no imminent influence on the failure mode. The moisture content determined on all specimens was between 10–12%.

For the analytical model, mean values were used. The mean values were derived from the characteristic values given in EN 14080 [4]. To derive the mean values, coefficients of variation given by the JCSS Probabilistic Model Code, Part 3: Resistance Models [5] were used.

The connectors for the experimental test campaign were manufactured using densified veneer wood (DVW). DVW is a glued laminated product, consisting of veneers impregnated with thermosetting synthetic resins, which are compressed in hydraulic presses under high temperature and pressure. Beech wood is the preferred veneer, as it is easy to impregnate, has high strength perpendicular to the veneers and is available in sufficient quantities. Thin veneers with thicknesses of 0.4–2.1 mm are predominantly used to allow for quick and even impregnation of the wood structure with synthetic resin. After the veneers have been assembled into packs, they are pressed at 100–250 bar and a temperature of 135–165 °C until the resin hardens. This produces panels with a bulk density of up to 1400 kg/m^3 [20,21].

The material properties of DVW were determined in tests with cross-laminated veneers [22]. Three different board thicknesses d = 6 mm, 10 mm and 15 mm were analysed. An excerpt of the results is shown in Table 1. The compressive strength and the modulus of elasticity in the plane of the panel, both decrease with increasing panel thickness. For connector plates with thickness greater 15 mm, the properties of 15 mm DVW were used and no further material tests were conducted. Alternative DVW products with different layups and veneer thicknesses were not included at this stage. These products, with increased material properties, would prevent failure of the connector itself. Therefore, they should be considered for future research.

To increase the friction in the shear plane, the surface of the connector plates was modified. In friction tests, coefficients of friction between softwood and modified surface were determined. Hereby, parameters such as fibre direction of the wood, contact pressure, and testing speed were varied. Subsequently, static and kinetic friction coefficients were evaluated. The different modification methods as well as the friction tests are presented in detail in [23]. The relevant friction coefficients for herein considered surfaces are given in Table 2 and exemplary surfaces can be seen in Fig. 1.

2.2. Connection tests (short-term)

Test specimens and programme. Push-out tests were carried out to determine the ultimate load-carrying capacity and the stiffness of connections with system connectors and inclined screws in insertion direction F_2 of the connectors, see Fig. 2. The connectors were made of DVW with modified surfaces. Each connection consisted of two connector plates, see Fig. 3. The connector plates were not mechanically connected. The load transfer between the two connector parts occurred via compressive contact. Table 2 provides an overview of all test series described in the following. The goal of series 1 was to determine whether inclined

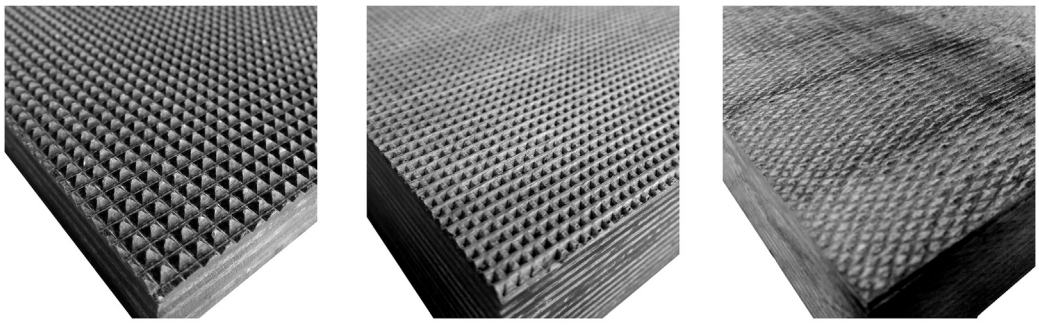

Fig. 1. Different modified surfaces: (a) milled pyramid pattern with milling depth of 1.5 mm. (b) embossed surface with imprint of pyramid pattern (penetration depth of embossing punch of approx. 1 mm). (c) milled circular pattern (depth of grooves approx. 0.5 mm)

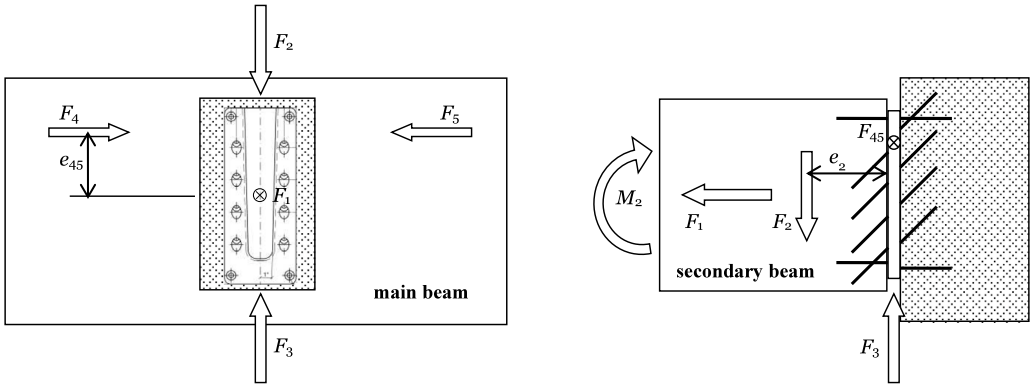

Fig. 2. Load directions for beam-to-beam connections with system connectors (in accordance to [24]).

Table 2
Overview of the short-term push-out tests with relevant static and kinetic friction coefficients for different surfaces (mean values).

Series	No. of tests	Surface	Coefficient of friction		Screw type and number	
			μ_{static}	$\mu_{kinetic}$		
1	3	Untreated	0.23	0.19	5 × 100	5
	3	Milled pyramids 1.0 mm	0.95	0.66	5 × 100	5
	3	Milled pyramids 1.5 mm	1.07	0.56	5 × 100	5
	3	Milled pyramids 2.0 mm	1.12	0.83	5 × 100	5
	3	Milled circular pattern	0.89	0.64	5 × 100	5
	3	Sanded	0.56	0.40	5 × 100	5
	3	Sandblasted	0.49	0.41	5 × 100	5
	3	Coated with EpoxyTape 0.1 mm	0.82	0.62	5 × 100	5
	3	Coated with EpoxyTape 1.0 mm	0.74	0.50	5 × 100	5
2	5	Milled pyramids 1.0 mm (offset)	0.95	0.66	5 × 100	5
	5	Milled pyramids 1.5 mm (offset)	1.07	0.56	5 × 100	5
3	5	Milled pyramids 0.5 mm	0.87	0.56	6 × 180	5
	5	Milled circular pattern	0.89	0.64	6 × 180	5
4	5	Untreated	0.23	0.19	6 × 100	15
	5	Embossed pyramid impression	0.79	0.52	6 × 100	15
	5	Milled pyramids 0.5 mm	0.87	0.56	6 × 100	15
5	3	Embossed pyramid impression	0.79	0.52	6 × 200	15
6a[a]	8	Milled pyramids 0.5 mm	0.87	0.56	6 × 200	10
6b[a,b]	7	Milled pyramids 1.0 mm	0.95	0.66	6 × 200	12
7[a]	5	Milled pyramids 1.0 mm	0.95	0.66	8 × 300	20

[a] Tests with prototype connectors.
[b] Analogous test series for long-term tests.

screws could generate sufficient contact pressure in the shear plane to activate the friction, and if the friction coefficients determined in [10] also occur in connections. Due to the wide range of surfaces tested and the preliminary nature of the tests, only three tests were performed on each surface. In subsequent test series 2 and 3, the position of the screws in the connector plate and the length of the screws were varied, and the number of tests was increased to five for each series to obtain more reliable data. The connectors in series 1–3 with 5 screws had a size of 110 × 58 mm^2, with two different thicknesses, 15 and 25 mm.

In series 4, the number of screws was increased to study the behaviour of connectors with closely spaced screw groups. The objective was to assess whether failure modes such as block shear failure needed

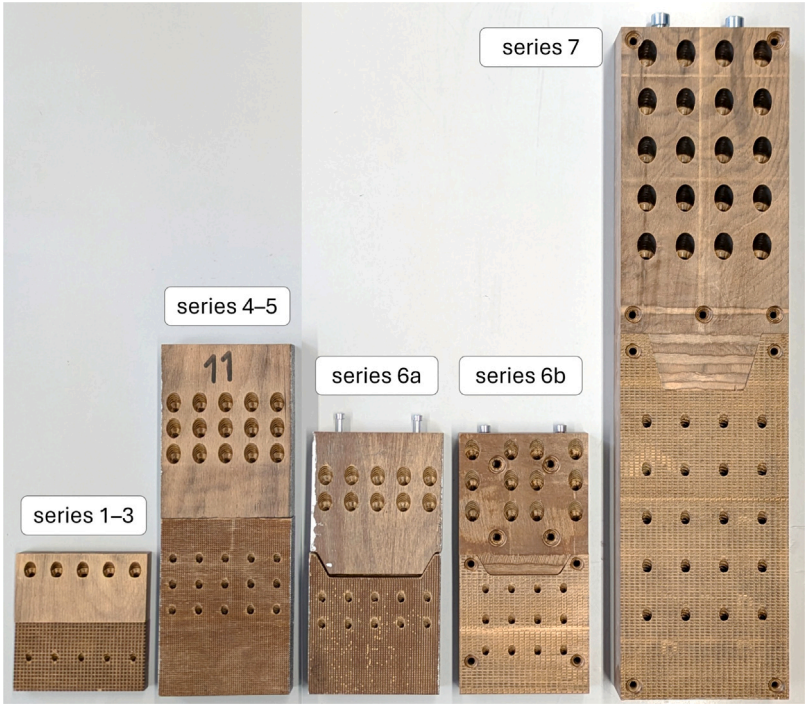

Fig. 3. Different connectors examined in push-out tests.

to be considered in future design models. Again, the length of the screws was varied in a further test series 5. The connectors with 15 screws were larger in size with 110 × 150 mm^2 and a thickness of 25 mm.

In series 6, prototype connectors were tested. The modified surface was a milled pyramid pattern: 0.5 mm deep for prototype v1 (series 6a) and 1.0 mm for prototype v2 (series 6b). Prototype v2 included four additional assembly screws inserted perpendicular to the shear plane to enhance fixation. Due to the occurrence of unexpected failure modes during the tests, the number of tests was increased to eight and seven, respectively.

In series 7, a heavy-duty prototype connector v3 was tested for loads up to 500 kN. Here, 20 inclined screws per connector plate were used. In series 6–7, the connector plates were connected with metric screws, but load transfer still relied on contact pressure. The metric screws ensure correct assembly and secure the connection against uplifting forces F_3 (Fig. 2). Therefore, they have no influence on the load capacity and stiffness in insertion direction F_2.

Table 2 provides an overview of all push-out tests, including the number of screws per connector plate and shear plane. Fig. 3 shows the examined connectors and highlights the size differences.

With the prototype connectors only, further tests were carried out to determine the load-carrying capacity F_1, F_{45} and M_2 (load and grain directions as shown in Fig. 2). The results of these tests are published in [10].

Test setup and execution. Fig. 4 shows the test setup for the push-out tests. The tests consisted of two outer members and one inner member. To avoid premature failure of the timber during the tests, the grain direction of the outer and inner members was parallel to one another. The DVW connectors were modified on one side only, and fastened to the outer and inner members with inclined screws at a 45° angle in all tests. Series 1–2 used fully threaded HECO-TOPIX screws [25] with a diameter of 5 mm. Series 3–7 used Würth ASSYplus VG 4 screws [26] with diameters 6 and 8 mm.

The inner members of the test specimens were loaded using a universal testing machine via a load cell and calotte, see Fig. 4. During testing, both the machine load and the relative displacement between the inner and outer members were recorded. Displacement was measured at the front and back of each connector. Series 1 used inductive displacement transducers (measuring rate of 5 Hz), while series 2–7 used a digital image correlation (DIC) system with a measuring rate of 1 Hz (LIMESS Messtechnik u. Software GmbH). Markers and LVDTs were placed on the timber at mid-height of the connector plates, see Fig. 4.

The test procedure followed EN 26891 [27] with unloading loop. For each connector, the maximum load $F_{2,\text{test}}$ and stiffness $K_{2,\text{ser,test}}$ were determined. The measured stiffness included deformation across both shear planes. The stiffness was evaluated in the linear-elastic range between 10 and 40% of the maximum load of each specimen.

2.3. Connection tests (long-term)

Test specimens and program. To investigate the behaviour of the connections with modified surfaces over time, long-term tests were performed. The fabrication of the test specimens followed the same procedure as for the short-term tests. Herein, only the tests with connector prototype v2 are presented and discussed. The test programme comprised duration-of-load (DoL) tests followed by the determination of the residual load-carrying capacity. Three specimens with two connections each were tested in two different climatic conditions: service class 1 (indoors and heated) and service class 2 (covered but open structure).

Test setup and execution. The experimental setup was based on the configuration used for the short-term tests and can be seen in Fig. 5. The constant load was applied via large compression springs in combination with threaded rods. The rods featured a metric thread M20 and strength class 10.9. Both inner members were loaded simultaneously and as uniformly as possible, using steel profiles and large washers. This arrangement enabled two push-out tests with four connectors to be conducted within a single system. Each compression spring provided a maximum force of 50 kN. The target load level was approximately 30% of the mean load-carrying capacity determined in the short-term tests. From a conservative perspective, the load level of approximately 30% corresponds to the upper limit of typical service loads. The test specimens were loaded with a universal testing machine up to 100 kN.

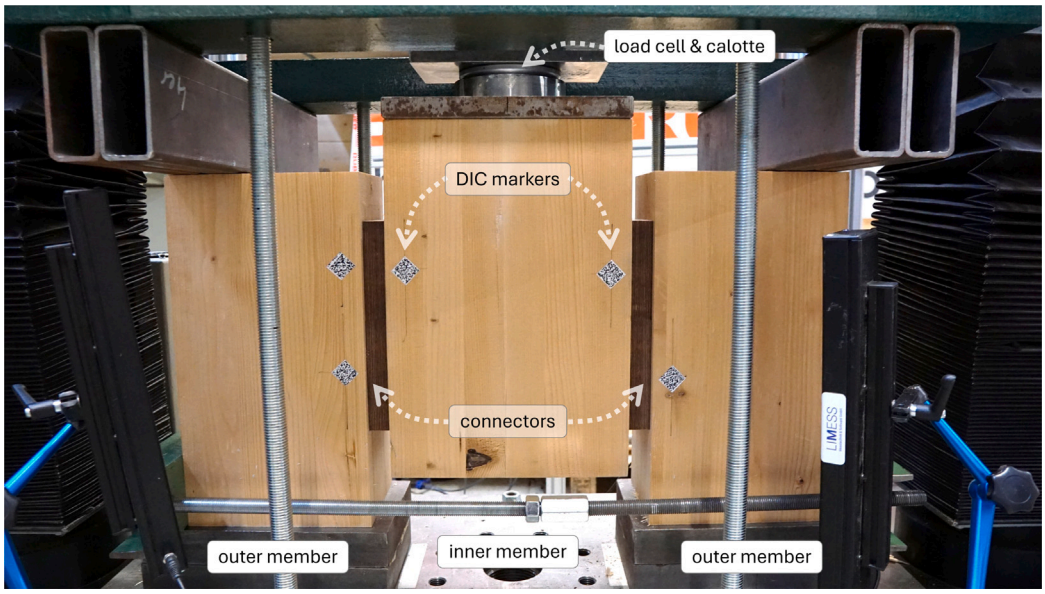

Fig. 4. Test setup for short-term push-out tests.

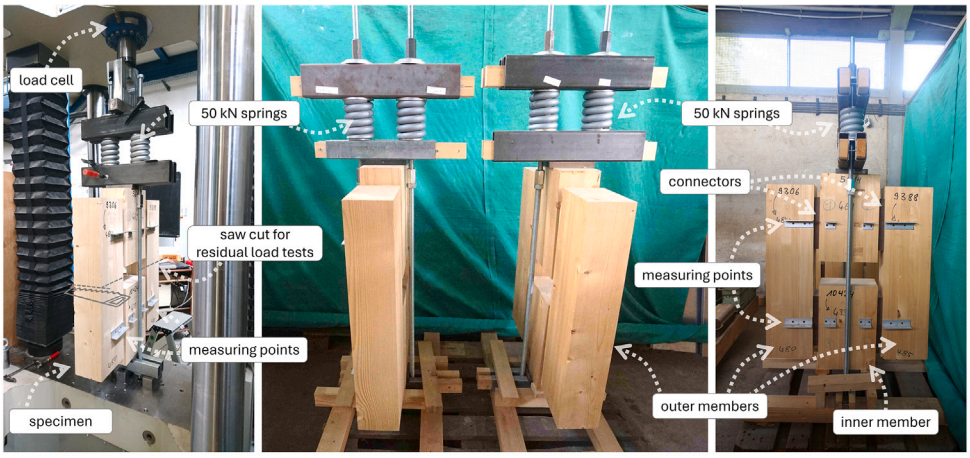

Fig. 5. Loading of specimen (a) and test setup of long-term tests (b+c).

The nuts of the threaded rods were then tightened, keeping the springs compressed at 50 kN.

The relative displacement between the outer and inner member was measured with a digital depth gauge in constant intervals. Subsequent to the reduction of the spring load to approximately 95% of the target load, the test specimens were returned to the laboratory to be reloaded. After ~570 days, the specimens were unloaded. The spring loads at that time were no less than 93% of the target load. The tests to determine the residual load-carrying capacity were performed analogous to Section 2.2.

Evaluation of creep factors. With the measured relative displacement, creep factors k_{def} were evaluated separately for both service classes. For the initial displacement to determine the creep factors, the displacement after 10 min was taken, in accordance with [28].

The creep factor is typically evaluated for a service period of 50 years. Therefore, the experimental test data was extrapolated, using two different models. A logarithmic model from [28] was adopted because it was specifically developed for timber-to-timber connections, see Eq. (1). Additionally, an exponential model from [29] was selected for its proven performance on timber in general, see Eq. (2).

$$k_{def}(t) = a \cdot log(1 + b \cdot t) \tag{1}$$

$$k_{def}(t) = a \cdot (1 - e^{-b \cdot \sqrt{t}}) \tag{2}$$

where
- t time in days
- a input parameter determined from test results
- b input parameter determined from test results

The input parameters a and b were determined with test data of 570 days for service class 1. For service class 2 test data of 330 days were used to determine the parameters, due to a better fit of the models.

To derive creep factors for application in EC5, the values reported in [28] were adjusted to ensure comparability. The modification is based on the condition that the predicted ultimate deformation must correspond to the experimentally measured ultimate deformation. To compare the creep factors for connections with inclined screws to other connections, the results were transformed using the same approach. The complete derivation is presented in [28]. The resulting creep factor is defined as follows:

$$k_{def,EC5} = \frac{K_{2,ser,model}}{K_{2,ser,10min}} \cdot (1 + k_{def}(t)) - 1 \tag{3}$$

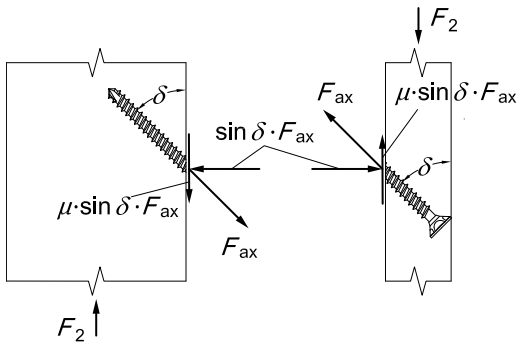

Fig. 6. Force diagram illustrating the acting forces in a connection with inclined screws.

where	$k_{def,EC5}$	proposed creep factor for EC5
	$k_{def}(t)$	predicted creep factor based on model
	$K_{2,ser,model}$	stiffness of connection based on model
	$K_{2,ser,10min}$	stiffness of connection after 10 min

The expected stiffness $K_{2,ser,model}$ was calculated with the herein presented spring model according to Eq. (30). The stiffness after 10 min $K_{2,ser,10min}$ was determined with the load of the respective load level and the measured displacement after 10 min.

2.4. Analytical model

An analytical model is introduced for both the load-carrying capacity and the stiffness of a connection with system connectors and inclined screws. To validate both models, the results are compared to the results of the tests with system connectors made of densified veneer wood (as presented in Section 2.2) as well as to results with aluminium connectors performed at the Research Centre of Steel, Timber and Masonry over the course of the last decade (source: unpublished test reports). The hereby used aluminium was of grade EN AW-6082 T6 (i.e. E = 70000 MPa [30]), and the screws were inclined by 45°.

2.4.1. Load-carrying capacity

Fig. 6 shows a connection with screws arranged at an inclination angle δ relative to the connector plane or shear plane. For equilibrium reasons, the horizontal component $\sin\delta \cdot F_{ax}$ of the axial screw force induces a compressive force perpendicular to the shear plane. This compressive force generates friction within the shear plane, commonly referred to as the *rope effect*.

For the design of screwed connections, the following failure modes should be considered, where the first three main failure modes govern: (1) Withdrawal failure, i.e. loss of the bond between the screw thread and the wood upon reaching the withdrawal capacity. (2) Tensile failure of the screw, i.e. rupture of the screw when its tensile capacity is exceeded. (3) Head pull-through failure, i.e. failure of the wood adjacent to the screw head when the head pull-though capacity is reached, causing the screw to be pulled through the wood on the head side. (4) Buckling failure of the screw. (5) Block shear failure along the circumference for groups of axially loaded screws. (6) Compressive failure of the timber beneath the connector plate upon reaching the compressive strength of the timber. (7) Failure of the connector itself upon reaching the strength properties of the connector material.

Failure modes (3), (4) and (5) are not included in the analytical model. Since the system connectors are made of steel, aluminium or densified veneer wood in this case, head pull-through is not critical because screw rupture occurs first. Buckling can be disregarded since the screws are subjected to tensile loading. Block shear failure did not occur during the tests with the DVW connectors and is, therefore, not regarded in the design model.

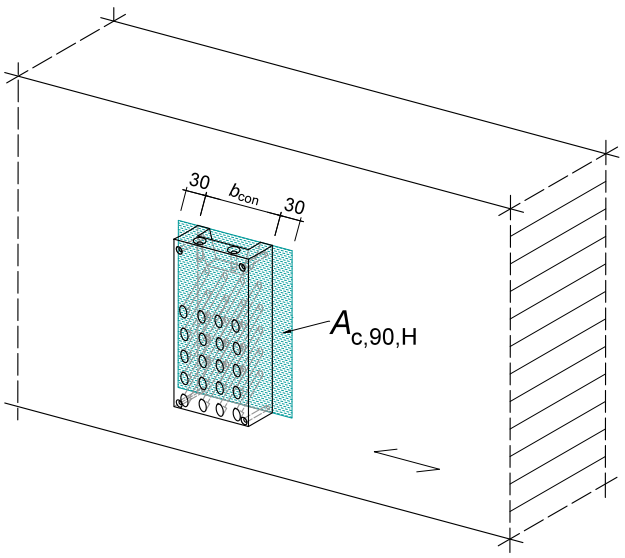

Fig. 7. Loaded area of the header $A_{c,90,H}$ beneath the connector plate.

The total load-carrying capacity for connections with connectors and inclined screws is governed by the minimum value from Eq. (4), where line 1 and 2 represent withdrawal and tensile failure, line 3 covers compressive failure perpendicular to the grain, and line 4 regards failure of the connector.

$$F_{2,R} = min\begin{cases} n_{ef} \cdot F_{ax,R} \cdot (\mu \cdot \sin\delta + \cos\delta) \\ n_{ef} \cdot F_{tens,R} \cdot (\mu \cdot \sin\delta + \cos\delta) \\ A_{c,90,H} \cdot f_{c,90,H} \cdot k_{c,90,H} \cdot \left(\mu + \frac{1}{\tan\delta}\right) \\ F_{2,con} \end{cases} \quad (4)$$

where	n_{ef}	effective number of fasteners
	$F_{ax,R}$	withdrawal capacity of a screw, in kN
	$F_{tens,R}$	tensile capacity of a screw, in kN
	μ	coefficient of friction
	δ	inclination angle of the screw with respect to the shear plane
	$A_{c,90,H}$	effective area under the connector plate at the header, in mm^2
	$f_{c,90,H}$	compressive strength perpendicular to the grain of the header, in N/mm^2
	$k_{c,90,H}$	coefficient for compression perpendicular to the grain
	$F_{2,con}$	load capacity of connector, in kN

The loaded area of the header $A_{c,90,H}$ includes 30 mm on each side in fibre direction, see Fig. 7. The capacities in Eq. (4) can either all be experimentally determined mean values or all be characteristic values, depending on the designer's needs.

Withdrawal capacity. To determine the short term mean withdrawal strength of fully threaded screws, Eq. (5) from [31] is used. The equation is based on over 700 tests and can be applied to self-drilling wood screws from all manufacturers, provided that their geometric properties are similar to those of the screws tested. To determine the characteristic withdrawal strength of fully threaded screws, Eq. (6) from the respective ETA is used [25,26].

$$F_{ax,Rm} = \frac{0.6 \cdot \sqrt{d} \cdot {l_{ef}}^{0.9} \cdot {\rho_m}^{0.8}}{1.2 \cdot \cos^2\alpha + \sin^2\alpha} \quad (5)$$

$$F_{ax,Rk} = \frac{k_{ax} \cdot f_{ax,k} \cdot d \cdot l_{ef}}{k_\beta} \cdot \left(\frac{\rho_k}{\rho_a}\right)^{0.8} \quad (6)$$

Table 3
Tensile and withdrawal strength of used screws.

Screw	5 × 100	6 × 100	6 × 200	8 × 300
Number of tests	12	12	15	5
$F_{tens,Rm}$ in kN	8.96	15.1	14.2	24.1
$F_{tens,Rk}$ in kN	7.90	12.5	12.5	22.0
$f_{ax,k}$ in N/mm^2	11.8	11.5	11.5	11.0

where d thread diameter, in mm
l_{ef} withdrawal length, in mm
$f_{ax,k}$ characteristic withdrawal parameter, in N/mm^2
k_{ax} 1.0 for $\alpha = 45°$
k_{β} 1.0 for glued laminated timber
ρ_m mean density, in kg/m^3
ρ_k characteristic density, in kg/m^3
ρ_a associated density, in kg/m^3
α angle between the fastener axis and the shear plane (as per ETA, equivalent to δ as per new EC5)

Tensile capacity. The tensile capacity of screws is dependant on the geometry and material of the screws. Mean values were determined experimentally within this study, and characteristic values are taken from the respective ETA (see Table 3).

Friction coefficient. In [23] friction coefficients for different surface modifications were determined. The evaluation showed that the mean kinetic friction coefficient μ_{kin} should be used to determine the load-carrying capacity of a connection in ultimate limit state. For the tests with the DVW connectors and modified surfaces the friction coefficients from [23] were taken, for the aluminium connectors, a friction coefficient of $\mu = 0.25$ according to Eurocode 5 (EC5) was assumed.

2.4.2. Stiffness - mechanical model with friction

In [11], a model was presented and investigated for the calculation of the stiffness of inclined screws loaded laterally (i.e. parallel to the shear plane). The resulting stiffness K_0 can be calculated from the stiffness of the screw in lateral (K_v) and axial direction (K_{ax}). This model has been adopted in the new generation EC5 [32], see Eq. (7), with the only changes that K_{ser} will be renamed to K_{SLS}.

$$K_{2,ser} = K_v \sin\delta(\sin\delta - \mu\cos\delta) + K_{ax}\cos\delta(\cos\delta + \mu\sin\delta) \quad (7)$$

where K_v lateral slip modulus
K_{ax} axial slip modulus
μ coefficient of friction
δ angle between the fastener axis and the shear plane

Lateral slip modulus. In [11,12] it is suggested to use the stiffness K_v of screws in lateral direction as specified in Table 7.1 of the current generation EC5 [33]. Eq. (8) gives the stiffness per fastener and shear plane.

$$K_v = \frac{\rho_m^{1.5} \cdot d}{23} \quad (8)$$

where d thread diameter, in mm
ρ_m mean density, in kg/m^3

The new generation EC5 [32] defines the lateral slip modulus dependant on the number of fasteners, see Eq. (9). The slip modulus of a connection depends on the number of fasteners in a row and the stiffness does not increase in proportion to the number of fasteners. Eq. (9) gives the stiffness of a connection.

$$K_{SLS,v} = \sum_{i=1}^{n_{90}} min\{n_{0,i}; 6\} \cdot m \cdot K_{SLS,v,i} \quad (9)$$

where n_0 number of fasteners in a row parallel to grain
n_{90} number of fasteners in a row perpendicular to grain
m number of shear planes per fastener
$K_{SLS,v,i}$ slip modulus of a single fastener per shear plane

The mean lateral slip modulus $K_{SLS,v,i}$ per fastener and shear plane is calculated according to Eq. (10) (from Table 11.12 in [32]).

$$K_{SLS,v,i} = 60 \cdot {d_1}^{1.7} \cdot \left(\frac{\rho_{mean}}{420}\right)^{1.1} \quad (10)$$

where d_1 inner thread diameter, in mm
ρ_{mean} mean density, in kg/m^3

In both, the current and new EC5, the values of mean lateral slip modulus should be doubled, for steel-to-timber connections, where the fastener is sufficiently clamped in the steel.

Axial slip modulus. The axial slip modulus can be seen as two springs placed in series, each with the stiffness $K_{ser,ax,i}$, see Eq. (11). This was proposed in [34] and adopted in [11].

$$K_{ax} = \frac{1}{\frac{1}{K_{ser,ax,1}} + \frac{1}{K_{ser,ax,2}}} \quad (11)$$

where $K_{ser,ax,i}$ axial slip modulus of the threaded part

For the axial stiffness of the threaded part of the screw, in [12] it is suggested to use either Eq. (12) from [35] or Eq. (13), which can be found in various ETAs [25,26]. However, Eq. (12) should no longer be used for determining the axial stiffness, as it results in too low values. Therefore, in [16], different test methods for the determination of the axial stiffness were used and analysed. Based on the test results, a test method was finally identified and a model was developed, see Eq. (14).

$$K_{ser,ax} = 234 \cdot (\rho d)^{0.2} \cdot l_{ef}^{0.4} \quad (12)$$

$$K_{ser,ax} = 25 \cdot d \cdot l_{ef} \quad (13)$$

$$K_{ser,ax} = 0.48 \cdot d^{0.4} \cdot {l_{ef}}^{0.4} \cdot \rho^{0.3} \quad (14)$$

where ρ mean density, in kg/m^3
d thread diameter, in mm
l_{ef} withdrawal length, in mm

The new generation of EC5 [32] adopts the double spring model for the axial slip modulus. For connections with dowel-type fasteners the mean axial slip modulus $K_{SLS,ax}$ per connected member should be be taken according to Eq. (15).

$$K_{SLS,ax} = n \cdot \frac{1}{\sum_{i=1}^{j} \frac{1}{K_{SLS,ax,i}}} \quad (15)$$

where n total number of fasteners
j total number of serially acting displacement shares
$K_{SLS,ax,i}$ mean slip modulus of displacement share i

The mean withdrawal slip modulus $K_{SLS,w,i}$ for the part of the fastener acting in withdrawal with the withdrawal length l_w limited to $20d$ is calculated according to Eq. (16) (from Table 11.13 in [32]).

$$K_{SLS,w} = 2 \cdot d^{0.6} \cdot {l_w}^{0.6} \cdot {\rho_{mean}}^{0.9} \quad (16)$$

where d diameter of the fastener, in mm
l_w withdrawal length, in mm
ρ_{mean} mean density, in kg/m^3

For the non-threaded part of the screw, the new EC5 suggests to use $K_{SLS,s}$, but does not further define $K_{SLS,s}$. Here, a spring constant of the part of the screw not acting in withdrawal is defined, as in Eq. (17).

$$K_{SLS,s} = \frac{EA}{l_s} \quad (17)$$

where EA tensile rigidity of screw
l_s screw length not acting in withdrawal

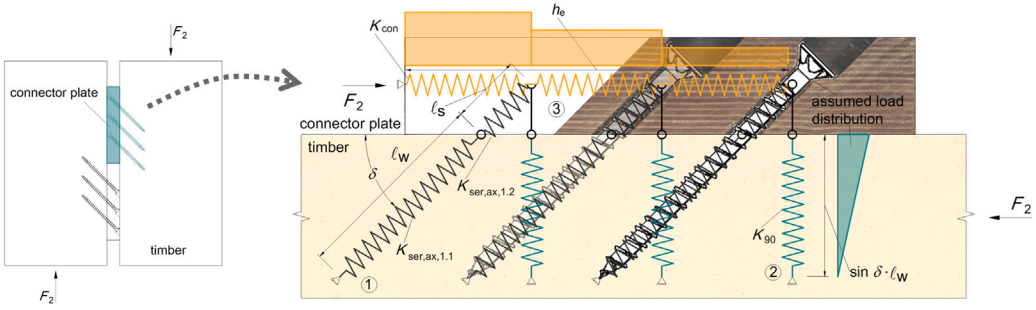

Fig. 8. Spring model for stiffness of connection.

Friction coefficient. In [23] it is concluded that the mean static friction coefficient μ_{stat} should be used to determine the stiffness of a connection in serviceability limit state. Again, the friction coefficients from [23] were taken for the tests with the DVW connectors and modified surfaces, and for the aluminium connectors $\mu = 0.25$ according to EC5 was assumed.

2.4.3. Stiffness - spring model without friction

This paper presents an alternative, more accurate design approach to the model in the new generation of EC5 [32]: a new spring-system model for determining the stiffness of connections with system connectors and inclined screws. Fig. 8 shows the herein presented spring model. When the connection is loaded (force F_2 parallel to the shear plane), the inclined screws react in tension to the external load. The stiffness of the screws is regarded by (1) a series connection of a spring covering the threaded part of the screw in the timber with the length ℓ_w and a spring covering the top part of the screw in the connector plate with the length ℓ_s. The axial load in the inclined screws leads to a load perpendicular to the shear plane, which is covered by (2) a compression spring perpendicular to the grain. It is assumed that this compression spring acts up to the level of the screw tips, with a length $\sin\delta \cdot \ell_w$. Furthermore, it is assumed that the compression load perpendicular to the grain beneath the connector plate decreases linearly up to the level of the screw tips. Finally, the connector itself is loaded in compression parallel to the shear plane, covered by (3) a compression spring in axial direction of the connector plate. It is assumed that the load distribution in the connector plates reduces at each row of screws resulting in a stepped distribution. This stepped distribution is further simplified with a linear decrease over the height of the connector h_e, i.e. the distance to the centre of the most distant loaded fastener.

The stiffness of the connection in the main loading direction F_2 can be determined using the principles of virtual work. The deflection of the connection follows Eq. (18).

$$w = \sum_{n=1}^{i} \frac{N_i \overline{N_i}\, l_i}{EA_i} = \sum_{n=1}^{i} \frac{N_i \overline{N_i}}{K_{ax,i}} \tag{18}$$

where

N_i		load in member i in specific load case
$\overline{N_i}$		load in member i in virtual load case
EA_i		axial rigidity of member i
l_i		length of member i
$K_{ax,i}$		axial stiffness of member i

To apply the principles of virtual work, the spring loads in both load cases are calculated.

$$N_1 = \frac{F_2}{\cos\delta} \tag{19}$$

$$N_2 = \frac{F_2 \sin\delta}{\cos\delta} \tag{20}$$

$$N_3 = F_2 \tag{21}$$

$$\overline{N_1} = \frac{1}{\cos\delta} \tag{22}$$

$$\overline{N_2} = \frac{1 \sin\delta}{\cos\delta} \tag{23}$$

$$\overline{N_3} = 1 \tag{24}$$

When inserting Eqs. (19)–(24) in Eq. (18), the displacement of the connection per shear plane can be determined.

$$w = \frac{F_2}{K_{ax,1}\cdot\cos^2\delta} + \frac{F_2 \sin^2\delta}{K_{ax,2}\cdot\cos^2\delta} + \frac{F_2}{K_{ax,3}} \tag{25}$$

$$w = F_2 \cdot \left(\frac{1}{K_{ax,1}\cdot\cos^2\delta} + \frac{\sin^2}{K_{ax,2}\cdot\cos^2\delta} + \frac{1}{K_{ax,3}} \right) \tag{26}$$

The stiffness K_{ser} of the connection can be calculated with Eq. (27).

$$K_{ser} = \frac{F_2}{w} = \frac{1}{\frac{1}{K_{ax,1}\cdot\cos^2\delta} + \frac{\sin^2\delta}{K_{ax,2}\cdot\cos^2\delta} + \frac{1}{K_{ax,3}}} \tag{27}$$

Axial stiffness of screw. The axial stiffness of the screw $K_{ax,1} = K_{ser,ax}$ is calculated according to Eq. (11), considering the slip modulus of the threaded part (Eqs. (13), (14) or (16)) and the slip modulus of the part in the connector plate (Eq. (17)).

Stiffness of timber in compression perpendicular to grain. The stiffness in compression $K_{ax,2}$ of the wood beneath the connector plate is calculated according to Eq. (28). For the compression stress, a linear declining behaviour is assumed along the perpendicular withdrawal length up to the level of the screw tips. It is assumed that the compressed area beneath each screw has a size of $a_1 \cdot a_2$, i.e. a_1 is the distance between screws parallel to the grain and a_2 is the distance between screws perpendicular to the grain.

$$K_{ax,2} = K_{90} = \frac{2\, E_{90}\cdot a_1 \cdot a_2}{\sin\delta \cdot l_w} \tag{28}$$

where

E_{90}		Modulus of elasticity perpendicular to the grain, in N/mm²
a_1		distance between screws parallel to the grain, in mm
a_2		distance between screws perpendicular to the grain, in mm
l_w		withdrawal length of inclined screw, in mm

For the modulus of elasticity perpendicular to the grain of glulam GL 24h a mean value of $E_{90} = 300$ MPa was chosen. For some tests with the DVW connectors, CLT was used instead of glulam. Here, the stiffness of the compression spring was calculated with an MOE of 11600 MPa, but only the area of the cross layers beneath the connector plate was taken into account. And finally, for the tests with DVW connectors and reinforced glulam beams, an equivalent MOE of 1000 MPa was used for the reinforced area, following test results in [35].

Stiffness of connector in compression. The stiffness in compression of the connector itself is calculated with Eq. (29). It is assumed, that the load distribution in the connector plates reduces at each row of screws resulting in a stepped distribution. This stepped distribution is further simplified with a linear decrease over the height of the connector

towards the lower/upper end of the connector plate. The height h_e is the distance to the centre of the most distant loaded fastener. The stiffness is calculated per connector plate and shear plane.

$$K_{ax,3} = K_{con} = \frac{2\,(EA)_{con}}{h_e} \tag{29}$$

where A_{con} area of connector subjected to compression, in mm^2
h_e distance to the centre of the most distant loaded fastener, in mm

Regarding the number of fasteners, a last adjustment has to be made. The axial stiffness of the inclined screws as well as the stiffness of the wood perpendicular to the grain is calculated per fastener. The compression stiffness of the connector plates, however, is calculated per shear plane. Therefore, the number of fasteners has to be considered only for $K_{ax,1}$ and $K_{ax,2}$, resulting in the total stiffness of the connection per shear plane as of Eq. (30).

$$K_{2,ser} = \frac{1}{\frac{1}{n_{ef}} \cdot \frac{1}{K_{ser,ax} \cdot \cos^2\delta} + \frac{1}{n_{ef}} \cdot \frac{\sin^2\delta}{K_{90} \cdot \cos^2\delta} + \frac{1}{K_{con}}} \tag{30}$$

3. Results and discussion

3.1. Connection tests

3.1.1. Short-term tests

Tests with 5 screws. The results of ultimate load and stiffness, along with their respective standard deviations, are given in Table 4. The corresponding load–displacement curves for all tests in series 1 can be seen in Fig. 9. Failure occurred either by withdrawal or rupture of the screws, i.e. failure modes (1) or (2), according to Section 2.4.1. In general the load-carrying capacity could be increased because of higher friction in the shear plane and, therefore, an additional load part parallel to the shear plane. This behaviour was especially pronounced with surfaces with protruding features, such as the milled pyramid pattern, see Fig. 1(a). This can be explained by the good interlocking of these surfaces with the softwood, see Fig. 12(a). The stiffness of the connections with these protruding surfaces, however, did not increase, and in some cases even decrease. For one, the deviation of the test results of the stiffness has to be considered, which was higher than for the ultimate loads. But also, due to the protruding features, the surfaces were further pressed into the softwood during the loading, leading to deformation perpendicular to the shear plane and, thus, lower stiffness values. The highest stiffness values were determined with surfaces with rather "flat" and even surfaces, such as untreated or embossed surfaces, see Fig. 1(b). Here, the even surface structures led to a tight fit of the surfaces and no additional deformation perpendicular to the shear plane. An increase in load-carrying capacity of tests with modified surfaces of 25–50% compared to tests with untreated surfaces was determined.

Tests with 15 screws. Based on the results, three surface conditions were tested: untreated DVW (reference), an embossed surface with a negative pyramid imprint, and a milled pyramid pattern (0.5 mm height). The results of ultimate load and stiffness are given in Table 4 (with their respective standard deviations). The corresponding load–displacement curves for all tests in series 4 can be seen in Fig. 10. Failure occurred by withdrawal of the screws, i.e. failure mode (1) according to Section 2.4.1. All surfaces exhibit initial linear behaviour; however, tests with untreated DVW flatten after 50% of ultimate load, whereas tests with modified surfaces maintain stiffness until 70–80%. The same observations as before are made for the different surfaces. Evaluation after the tests revealed no group effect in the form of block shear failure. This is also evident in the results, which show an almost linear increase in load-carrying capacity from tests with five screws to those with 15 screws. Also, the screw arrangement distributed the contact pressure evenly, see Fig. 12(a). Series 4 confirmed previous findings: protruding features of the surface increased load capacity by up to 30%, while uniform surfaces improved stiffness by up to 30%. Failure occurred by screw withdrawal. For the first time, large deformations perpendicular to the shear plane were observed during the tests, see Fig. 12(b). Based on these tests, the failure of the wood perpendicular to the grain beneath the connector plate was included in the analytical model.

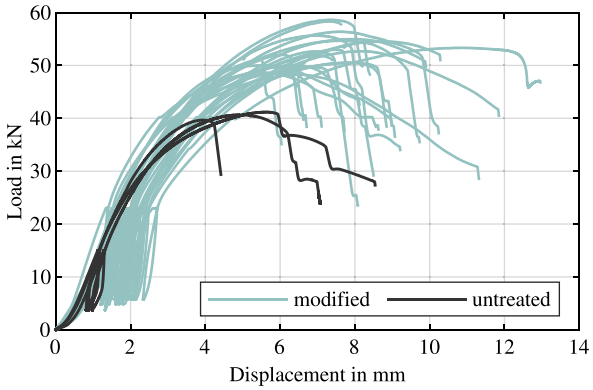

Fig. 9. Load–displacement curves for series 1. Comparison of untreated (black) to modified surfaces (teal).

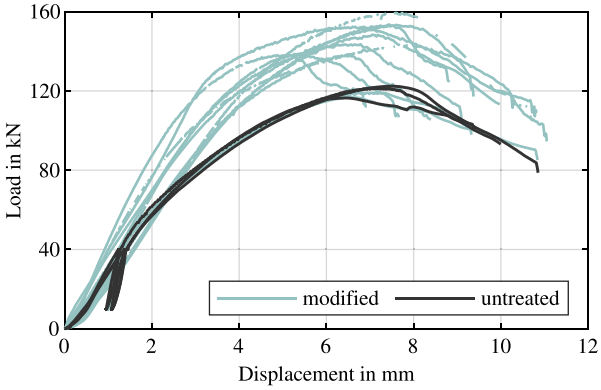

Fig. 10. Load–displacement curves for series 4. Comparison of untreated (black) to modified surfaces (teal).

Tests with prototype connectors. The tests with the prototype connectors confirmed the feasibility of DVW connectors as an alternative to conventional system connectors. The ultimate load and stiffness results are given in Table 5 with their respective standard deviations. Failure occurred mainly by rupture of the screws for the tests with connector v1 (failure mode (2) according to Section 2.4.1). The total load of the prototype connectors could be increased from v1 to v2. With the higher loads in the tests of connector v2, again, failure of the wood perpendicular to the grain became decisive (failure mode (6) according to Section 2.4.1), leading to additional tests with reinforcement screws placed beneath the connector plates, and tests with CLT. 5-ply CLT was used with two cross layers perpendicular to the shear plane acting as natural reinforcement. Both adaptations of the specimens excluded failure perpendicular to the grain, enabling the connectors to reach their full capacity. The load–displacement curves for all tests with prototype connectors can be seen in Fig. 11, showing the differences between prototype v1 (gold) and v2 (teal), as well as the differences in the specimens' reinforcements in the tests with prototype v2. Where applicable, one example from each series is shown in dark colour, while the rest are shown in a light colour.

Table 4
Ultimate loads and stiffness values from the tests of series 1 and 4 (mean values).

Surface	Series 1		Series 4	
	$F_{2,test}$ in kN	$K_{2,ser,test}$ in kN/mm	$F_{2,test}$ in kN	$K_{2,ser,test}$ in kN/mm
Untreated	40.5 ± 0.8	16.7 ± 0.9	119 ± 3	33.5 ± 2.7
Embossed	–	–	140 ± 3	42.6 ± 9.0
Milled pyramids 0.5 mm	–	–	153 ± 4	34.0 ± 3.5
Milled pyramids 1.0 mm	52.9 ± 4.0	15.6 ± 0.8	–	–
Milled pyramids 1.5 mm	53.4 ± 1.3	12.2 ± 0.7	–	–
Milled pyramids 2.0 mm	52.8 ± 2.1	11.0 ± 1.0	–	–
Milled circular pattern	49.9 ± 0.2	14.7 ± 1.4	–	–
Sanded	50.3 ± 1.6	16.3 ± 3.0	–	–
Sandblasted	50.6 ± 1.7	17.9 ± 2.5	–	–
Coated with EpoxyTape 0.1 mm	57.8 ± 1.2	13.6 ± 0.7	–	–
Coated with EpoxyTape 1.0 mm	52.3 ± 2.4	11.4 ± 0.7	–	–

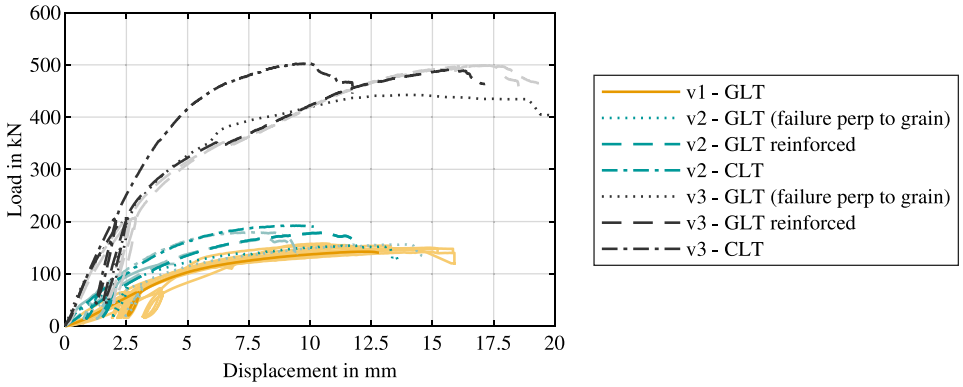

Fig. 11. Load–displacement curves for series 6 and 7. Comparison of prototype v1 (gold), prototype v2 (teal) and prototype v3 (black).

Table 5
Ultimate loads and stiffness values from the tests of series 6 and 7 (mean values).

Series	Prototype	Timber	Surface	Number of tests	$F_{2,test}$ in kN	$K_{2,ser,test}$ in kN/mm
6	v1	GLT	Milled pyramids 0.5 mm	8	151 ± 5	25.0 ± 4.0
	v2	GLT[a]	Milled pyramids 1.0 mm	2	156 ± 2	30.3 ± 3.3
	v2	GLT[b]	Milled pyramids 1.0 mm	2	173 ± 9	33.3 ± 2.4
	v2	CLT	Milled pyramids 1.0 mm	2	186 ± 9	63.5 ± 8.7
7	v3	GLT[a]	Milled pyramids 1.0 mm	1	443	82.0
	v3	GLT[b]	Milled pyramids 1.0 mm	3	496 ± 4	80.9 ± 4.3
	v3	CLT	Milled pyramids 1.0 mm	1	503	105

[a] Compressive failure perpendicular to the grain of the softwood members.
[b] Softwood members reinforced with fully threaded screws.

In the first test with prototype v3, failure due to compression perpendicular to the grain occurred. Subsequent tests reinforced the softwood with fully threaded screws (8 × 160 mm), countersunk to allow the pyramid pattern to press into the wood, see Fig. 12(c). Failure then occurred mainly by compression failure of the connector plate parallel to the grain, and one test reached the screw's tensile capacity. As before, a last test was performed with CLT, resulting in the same ultimate load, but leading to higher stiffness. As previously, 5-ply CLT was used with two cross layers perpendicular to the shear plane acting as natural reinforcement. The load–displacement curves for all tests in series 7 are also given in Fig. 11 (black). Again, one exemplary test is plotted in dark colours, while the other tests of the series are plotted in light colours. The CLT specimen stands out due to its significantly increased stiffness:

It should be noted that some of the presented test series are based on a limited number of specimens. The main reasons are stated in Section 2.2. As a result, the statistical robustness of these subsets is limited, and the observed trends should be interpreted with appropriate caution.

3.1.2. Long-term tests

Residual load-carrying capacity. After unloading, the specimens were cut in half along the cut line shown in Fig. 5(a) and the residual load-carrying capacity was determined. The results are given in Table 6 and load–displacement curves are shown in Fig. 13.

Service class 1. A mean ultimate load of about 84% of the short-term tests was reached. The reduced capacity likely stems from limited sample size, and time-dependant timber property reduction [36]. Also, the screws may have reached their deflection limits before their load capacity was reached. This explanation is consistent with findings of tests on combined bending and axial loads in [37]. The load–displacement curves start softer and flatten earlier, with tensile failure of the inclined screws at slightly larger displacements (all compared to the short-term tests). The initial slip of the connections may result from timber shrinkage and elastic recovery of the screws after unloading of the springs. Despite this, stiffness between 10–40% of ultimate load was about 7% higher than in the short-term tests. The increased stiffness can be attributed to the constant loading over time, which pressed the pyramid pattern firmly into the softwood. Unlike with

Table 6
Results of residual load-carrying capacities in different climatic conditions compared to short-term tests.

	Short-term[a] (n = 2)				SC 1 (n = 3)				SC 2 (n = 3)			
	$F_{2,test}$ [kN]	w_{max} [mm]	$K_{2,ser,test}$ [kN/mm]	u [%]	$F_{2,test}$ [kN]	w_{max} [mm]	$K_{2,ser,test}$ [kN/mm]	u [%]	$F_{2,test}$ [kN]	w_{max} [mm]	$K_{2,ser,test}$ [kN/mm]	u [%]
MEAN	173	9.48	33.3	11.3	145	11.1	35.7	11.0	154	11.8	36.4	15.2
SD	8.5	1.46	2.4	0.5	4.1	1.22	3.0	0.2	0.7	0.38	4.6	0.5
COV	5%	15%	7%	4%	3%	11%	8%	2%	0%	3%	13%	3%

[a] Tests without compressive failure perpendicular to the grain of the softwood members.

(a) (b) (c)

Fig. 12. Imprint of modified surface in softwood, showing good interlocking (a). Failure of wood perpendicular to the grain beneath the connector plate (b). Countersunk reinforcement screws beneath the connector plates (c).

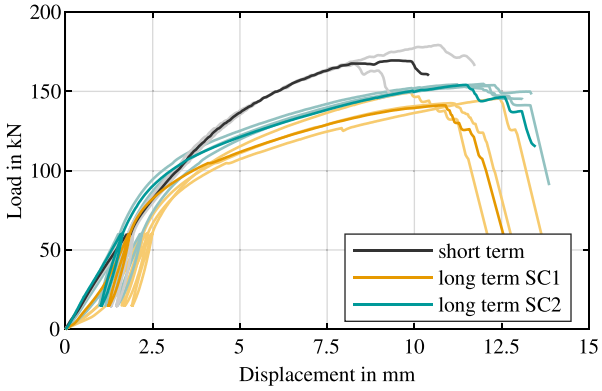

Fig. 13. Load–displacement curves of residual load for connectors in SC 1 (gold) and connectors in SC 2 (teal).

the short-term tests, no deformations perpendicular to grain occurred, allowing full interlocking and higher stiffness. The results show that sufficient contact pressure can be created in the shear plane even after an extended time under constant load. This was also confirmed by a close inspection of the friction area after the tests, where a good surface interlocking was visible.

Service class 2. The tests in SC 2 achieved a mean load of about 90% of the short-term tests. Again, the reduction in load-carrying capacity might rather be attributed to reduced mechanical properties of the timber, than to a loss of friction over time. The load–displacement curves show a stiff initial behaviour but still flatten earlier, with tensile failure of the inclined screws at slightly larger displacements. This is confirmed by the evaluation of the stiffness, which was 10% higher than in the short-term tests. Possible explanations for the reduced ultimate loads and increased stiffness mirror the findings from the tests in SC 1. Overall, the results in SC 2 exceed the results in SC 1 in both load and stiffness, likely due to swelling of the wood, thus, improving the interlock of the pyramid pattern and the softwood, eliminating initial slip. The failure modes remained consistent with the short-term tests. The evaluation of the results show that the modified surface and the contact with the softwood was not affected by the changing environmental conditions and the constant load.

Table 7
Different models for creep and their input parameters for different climatic conditions.

Model	a	b	R^2	Climate
Logarithmic model	0.300	0.118	0.85	SC 1
	0.400	0.039	0.99	SC 2
Exponential model	0.725	0.059	0.81	SC 1
	2.130	0.014	0.99	SC 2

Creep factor. The creep factor k_{def} was evaluated separately for both service classes with the relative displacement. The resulting creep factors over time for the test period are plotted in Fig. 14.

As the exponential model tends towards a horizontal asymptote, and the logarithmic model predicts a continued deformation, it is difficult to make a reliable long-term prediction from the limited data set. Therefore, the results should be interpreted with caution, and the predicted creep factors should serve as lower and upper bounds. Also, the recorded data includes creep contributions from both the timber and the DVW, which may influence the results. Dedicated measurements of both materials would allow for a more accurate assessment of the creep contributions. Both models are described with two unknown parameters, a and b. These parameters were calibrated for the time t expressed in days and are given in Table 7.

For both service classes the connections show typical behaviour with an initial sudden increase in deformation and then a gradual increase over time, see Fig. 14. No direct correlation was observed between the environmental conditions and the deformation, i.e. the deformation did not exhibit a sudden increase or decrease in response to changes in relative humidity or temperature. Jumps in the curves likely stem from measurement inaccuracies with the depth gauge setup. No smoothing, filtering or outlier treatment was applied before fitting the creep models. The displacement after 10 min was consistent with the short-term results. The dashed and dotted lines in Fig. 14 represent the two models, and show a good fit to the test data. The results show that both models reproduce the available test data with comparable accuracy.

Table 8
Creep factors for different load durations for single-shear connections with inclined screws and modified surfaces. Due to the limited dataset, the values should be interpreted as preliminary.

Load duration	Time	Creep factor $k_{def,EC5}$			
		screws SC 1[a]	screws SC 2[a]	nails SC 1[b]	TCC SC 1[c]
Permanent	50 years	1.1	1.4	4.3	2.1
Long term	10 years	1.0	1.0	3.2	1.9
Medium term	6 months	0.6	0.3	1.1	0.7

[a] Tested herein.
[b] Results from [28].
[c] Results from [38].

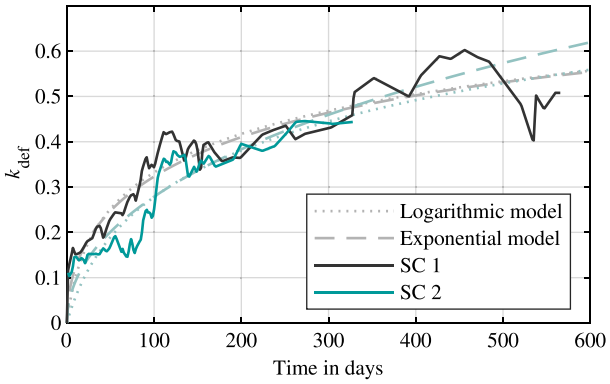

Fig. 14. Creep factor k_{def} for 570 days in service class 1 (black) and 330 days in service class 2 (teal).

The modified creep factors $k_{def,EC5}$ according to Eq. (3) are given in Table 8 for different load durations. The results are compared to values from literature for timber-to-timber connections with nails [28] and timber-concrete composites (TCC) with dowel-type fasteners [38]. The creep factors estimated for connections with inclined screws are approximately 50% lower than those for connections using nails or other dowel-type fasteners. A direct comparison of the values is somewhat misleading, as connections with axially loaded fasteners are being compared to connections with laterally loaded fasteners. So the results seem reasonable as the axial stiffness of dowel-type fasteners exceeds the lateral stiffness and thus the deformation of the two different connection types differ.

The influence of the modified surface and the increased friction in the shear plane can be seen for the medium term load duration. In SC 1 the pronounced structure of the modified surface is still being pressed into the softwood member, leading to greater deformation and a greater creep factor. Whereas in SC 2, a swelling of the softwood member accelerates the complete interlocking of the modified surface, which results in smaller deformation and thus a smaller creep factor. As no tests with untreated surfaces were performed, it is currently not possible to discuss the contribution of increased friction in the shear plane separately. In general, further research needs to be conducted on the long-term behaviour of connections with inclined screws, as the herein presented data set is limited.

3.2. Analytical model

3.2.1. Load-carrying capacity

The load-carrying capacity of each connection was calculated with Eq. (4) from Section 2.4, with the effective number of fasteners according to Eq. (31) from the respective ETA.

$$n_{ef} = max\{n^{0.9}; 0.9 \cdot n\} \tag{31}$$

The ultimate loads from the tests are first compared to the average load-carrying capacities, see teal markers in Fig. 15. For the tests with aluminium connectors, $\mu = 0.25$ was used, see Fig. 15(a). For the tests with the DVW connectors, μ was used according to the results of the friction tests with the modified surfaces, as given in Table 2. Here, it was further distinguished between the static and the kinetic friction coefficient, see Fig. 15(b). Additionally, characteristic values were derived from the test results for each series and compared to the characteristic load-carrying capacities according to the model, see grey markers in Fig. 15.

Table 9
Characteristic ratios $F_{2,test}/F_{2,Rk}$ for different friction coefficients μ.

Series	n	μ_{EC5}	μ_{stat}	μ_{kin}
Aluminium	156	1.12	–	–
DVW	180	–	0.92	1.13

In a second step, it was determined whether the model is sufficiently conservative for the application. For a conservative assessment of the load-carrying capacity, the characteristic ratio $F_{V,test}/F_{V,Rk}$ should be greater than 1.0. The 5th-percentile was determined according to EN 14358 [39], assuming a log-normal distribution. The evaluation determines a ratio of 1.12 for the aluminium connectors and a ratio of 0.92–1.13 for the DVW connectors, depending on the coefficient of friction. The static coefficient leads to a non-conservative prediction, whereas the kinetic coefficient provides a conservative characteristic assessment.

Table 9 shows all characteristic ratios for the load-carrying capacity. The evaluation shows that the model predicts the load-carrying capacity of aluminium connectors quite well when a friction coefficient of $\mu_{EC5} = 0.25$ is used. For DVW connectors with modified surfaces and increased friction in the shear plane, the model predicts the load-carrying capacity accurately when the kinetic friction coefficient is used, whereas for the static coefficient of friction the characteristic ratio is smaller than 1.0. This supports the conclusion in [23] to use the kinetic friction coefficient for design in ultimate limit state.

3.2.2. Stiffness

The comparison of test results to model results can be seen in Fig. 16. First, the mechanical model according to the new generation of EC5 [32] was evaluated. The stiffness per shear plane and connector plate was calculated according to Eq. (7), with both the lateral and axial slip modulus determined according to the equations in the new generation EC5 (gold markers). In comparison, the same Eq. (7) was used to determine the total stiffness per shear plane and connector plate, but it was differentiated between the lateral slip modulus according to the current EC5 in combination with the axial slip modulus according to ETA [25,26] (black markers) or the axial slip modulus according to [16] (teal markers). The results show that with all three combinations of lateral and axial slip modulus, the stiffness of the connection under loading parallel to the shear plane is overestimated. Mean ratios of K_{test} / K_{model} range from 0.3–0.7, thus, being significantly smaller than 1.0.

One possible explanation for this is that the model neglects deformation perpendicular to the shear plane. That this deformation

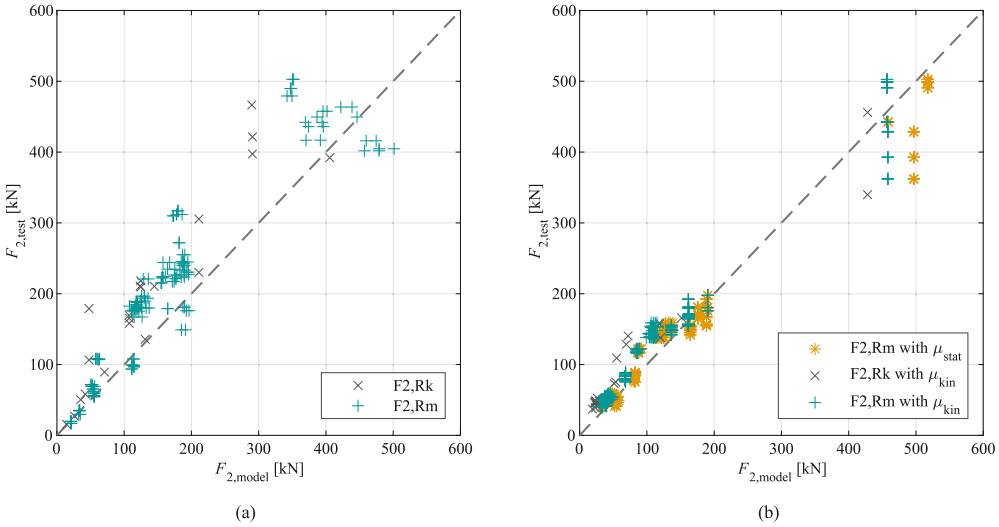

Fig. 15. Comparison of F_{test} with F_{model} for (a) aluminium connectors and (b) DVW connectors. Each marker represents a connection consisting of two connector plates.

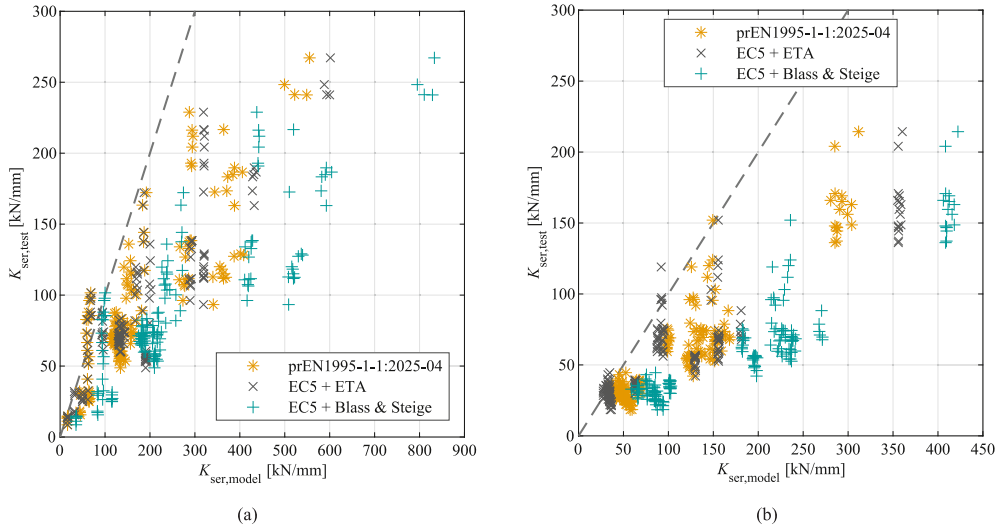

Fig. 16. Evaluation of mechanical model: comparison of K_{test} with K_{model} for (a) aluminium connectors and (b) DVW connectors (determined with Eq. (7) and $n_{ef} = n^{0.9}$). Each marker represents a stiffness per connector plate and shear plane.

occurs during testing was shown in [23] especially for connectors with modified surfaces where displacement parallel to the shear plane led to further impression of the modified surface into the softwood, see also Fig. 12(b). Therefore, the spring model was developed, see Section 2.4.3. Here, compression springs beneath each screw allow for deformation perpendicular to the shear plane and thus an analytical reduction of the stiffness. However, the influence of friction is neglected.

The evaluation of the spring model shows an adequate fit to the test results, considering the generally high scatter when determining the stiffness, which was also documented in [13,15]. For both connector types, i.e. aluminium connector plates without modification and DVW connector plates with modified surfaces, the results align with the identity line ($K_{test} = K_{model}$), see Fig. 17. Also, it is shown that the differences in the various design equations for the lateral and axial slip modulus are no longer as pronounced as before. This confirms that deformations perpendicular to the grain contribute significantly to the total stiffness and, therefore, have to be considered analytically. Furthermore, the conclusion in [23] that increased friction in the shear plane does not increase the stiffness to the same extent than the load-carrying capacity is confirmed.

Table 10
Mean ratio $K_{ser,test}/K_{ser,model}$ for different design equations of $K_{ser,ax}$.

Series	n	ETA	Blass & Steige (2018)	FprEN 1995-1-1:2025-04
Aluminium	154	1.89	1.58	1.78
DVW	172	2.03	1.49	1.75

To assess the goodness of the model, the ratio $K_{ser,test}/K_{ser,model}$ should be close to 1.0. The values range between 1.58–1.89 for the aluminium connectors, depending on the design equation for the axial slip modulus. For the DVW connectors, the values range between 1.49–2.03, again, depending on the axial slip modulus. All ratios are given in Table 10.

It can be seen that the compressive stiffness perpendicular to grain has a major impact on the stiffness of the connection. The spring model significantly reduces the scatter of the results, especially for the aluminium connectors. A closer look at the compressive stiffness

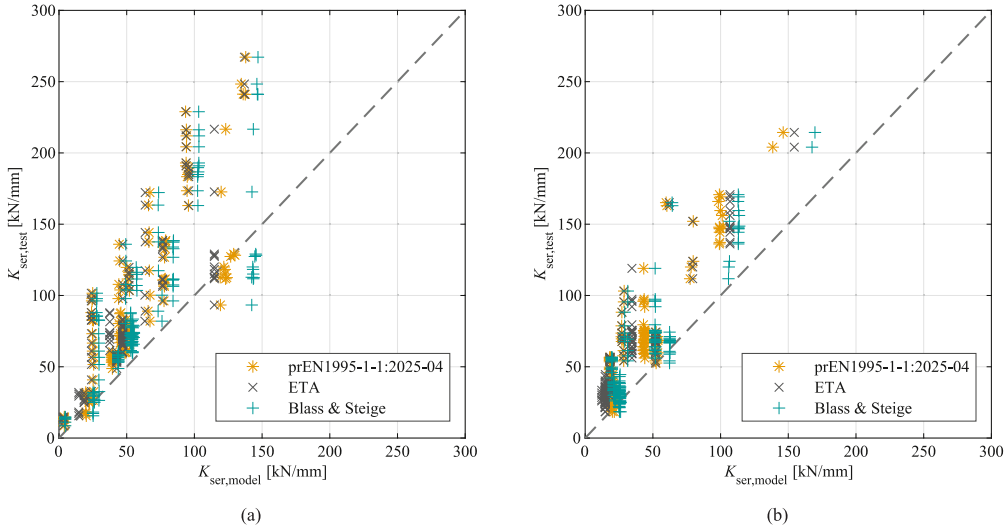

Fig. 17. Evaluation of spring model: comparison of K_{test} with K_{model} for (a) aluminium connectors and (b) DVW connectors (determined with Eq. (30) and $n_{ef} = n$). Each marker represents a stiffness per connector plate and shear plane.

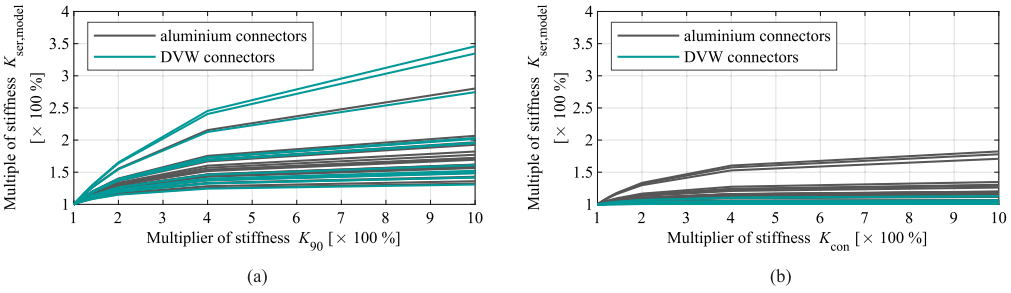

Fig. 18. Influence of (a) the stiffness K_{90} and of (b) the stiffness K_{con} on the connection stiffness $K_{ser,model}$.

perpendicular to grain reveals that the assumption of the length of the spring has a major influence on the results, i.e. the assumption that the compressive forces perpendicular to grain decreases up to the level of the screw tips.

If this length is reduced, the spring constant increases by the reciprocal of the reduction. This has a significant influence on the stiffness of the connection, see Fig. 18(a). For example, reducing the effective length of the compressive strength perpendicular to grain to $0.9 \cdot \ell_w$ (equivalent to an increase in the stiffness in compression perpendicular to grain by a factor of 1.1) already leads to an increase in connection stiffness of up to 10% (both aluminium and DVW). Halving the effective length, i.e. doubling the compressive stiffness, results in an increase in connection stiffness of 15–40% (also aluminium and DVW). However, there are also outliers in both connector groups with increases of between 55–75%.

The evaluation of the data suggests that the assumption of the spring length of the compression spring perpendicular to grain up to the level of the screws' tips (in combination with small distances between the screws, a_1 and a_2) is conservative. It seems that the compressive stresses perpendicular to grain beneath the connector plates subside earlier.

If the compressive strength of the connectors is analysed to the same extent and the assumption of the effective length of the connector spring is checked, a different picture shows, see Fig. 18(b). If only 90% of the effective height of the connector plate is taken into account (corresponding to an increase in connector stiffness in compression by a factor of a 1.1), the connection stiffness increases by only 5% (aluminium) and 2% (DVW). By halving the effective length (doubling the connector stiffness), the overall stiffness increases by up to 20% for aluminium connectors up to a height of 400 mm and by up to 30% for connectors with a nominal height of 600 mm.

For DVW connectors, the increase in overall stiffness is up to 10% for all connector heights. This shows that the assumption of a stepped load distribution and the simplification with a linear decline is sufficiently accurate and that a more dedicated consideration of the spring length would only minimally change the model results.

4. Conclusions

Load-carrying capacity. The experimental test campaign showed that increasing friction in the shear plane through surface modification can significantly increase the total load-carrying capacity of connections with inclined screws; a more pronounced surface structuring leads to a higher friction coefficient and consequently to a higher ultimate load.

Although the residual load after a longer period of constant loading decreased slightly, this reduction is attributed to the degradation of material properties (i.e. duration of load) rather than to a loss of friction. Moreover, the deformation analysis revealed that the creep factors for inclined screws are only a fraction of those for other dowel-type fasteners in shear. Due to the limited data available, it is not yet possible to determine the optimal surface structure for long-term performance.

The analytical model predicts the load-carrying capacity reliably; when modified surfaces are considered, the kinetic coefficient of friction should be used. These findings enable engineers to bring densified veneer wood connectors with modified surfaces from research to practice as a sustainable alternative to aluminium connectors, combining improved mechanical performance with enhanced fire resistance and environmental benefits.

Stiffness. The tests demonstrated that increasing friction in the shear plane through surface modification yields only a marginal increase in connection stiffness. Here, further impression of the modified surface into the softwood counter acted the ability to increase the stiffness. Therefore, it can be concluded that flat and evenly structured modified surfaces are most effective for increasing stiffness, as confirmed by the tests.

Long-term tests indicated that maintaining a constant load over time further improves stiffness because the modified surface becomes fully interlocked with the softwood. Moreover, the results show that climate-induced swelling and shrinkage do not adversely affect stiffness for connections that combine modified surfaces with inclined screws.

The analytical assessment revealed that the mechanical model adopted in the new generation EC5 [32] is unsuitable for predicting the stiffness of connections with inclined screws and system connectors, because it neglects deformations perpendicular to the grain beneath the connector plate, leading to substantial over-estimation of stiffness values. In contrast, the spring model introduced herein accurately accounts for compression deformation perpendicular to the grain, providing more reliable stiffness predictions for various timber components, including cross-laminated timber and glued-laminated timber reinforced with fully threaded screws. For practical design, engineers should prioritize surface modifications for strength rather than stiffness and apply the proposed spring model for more accurate serviceability assessments.

CRediT authorship contribution statement

Simon Aurand: Writing – review & editing, Writing – original draft, Visualization, Validation, Software, Resources, Methodology, Investigation, Formal analysis, Data curation, Conceptualization. **Hans Joachim Blass:** Writing – review & editing, Supervision, Project administration, Methodology, Funding acquisition, Conceptualization.

Declaration of competing interest

The authors declare that they have no known competing financial interests or personal relationships that could have appeared to influence the work reported in this paper.

Acknowledgements

The authors acknowledge the financial support for parts of the work from the Association of Industrial Research Associations (AiF) in form of the "Central Innovation Programme for small and medium-sized enterprise" (ZIM ZF4250805WZ). Pitzl Connectors is acknowledged for providing the prototype connectors, Würth and HECO are acknowledged for providing the self-tapping screws used in the study. Last but not least, Prof. Philipp Dietsch of KIT Timber Structures and Building Construction is acknowledged for supporting the research and reviewing the final draft.

Data availability

Data will be made available on request.

References

[1] Eichhorn Sven, Kluge Patrick, Penno Eric, Eckardt Ronny, Müller Christoph, Feig Katrin, Alt Christoph, Schubert Christine. SubSTANCE – Substitution of energy-intensive Steel- and Aluminum materials by reNewable resources in Conveyor Engineering. 2017, TU Chemnitz, Professur Fördertechnik.

[2] Brandon Daniel, Maluk Cristian, Martin P Ansell, Harris Richard, Walker Pete, Bisby Luke, Bregulla Julie. Fire performance of metal-free timber connections. Proc Inst Civ Eng - Constr Mater 2015;168(4):173–86. http://dx.doi.org/10.1680/coma.14.00055.

[3] Haller Peer, Hamann Martin, Hofmann Mathias. Hochleistungsholztragwerke - HHT - Entwicklung von hochbelastbaren Verbundbauweisen im Holzbau mit faserverstärkten Kunststoffen, technischen Textilien und Formpressholz: Abschlussbericht zum BMBF-Forschungsvorhaben 0330722A-C. Dresden: Institut für Stahl- und Holzbau; 2011, http://dx.doi.org/10.2314/GBV:669133302.

[4] EN 14080:2013-09. Timber structures – Glued laminated timber and glued solid timber – Requirements; German version. Berlin: DIN Deutsches Institut für Normung e. V. 2013.

[5] JCSS PMC. JCSS Probabilistic Model Code (periodically updated, online publication). 2001, Joint Committee on Structural Safety.

[6] Bejtka Ireneusz, Blass Hans Joachim. Joints with inclined screws. In: Proceedings of CIB W18 - meeting 35. Kyoto, Japan; 2002, paper 35-7-4.

[7] Krenn Harald. Die Stahlblech-Holz-Laschenverbindung mit schrägen Schrauben. [Ph. D. thesis], Monographic series TU graz/timber engineering & technology, vol. 7, Graz: Verlag der Technischen Universität Graz; 2018, http://dx.doi.org/10.3217/978-3-85125-622-2.

[8] Dorn Michael. Investigations on the serviceability limit state of dowel-type timber connections. [Ph. D. thesis], Wien: Fakultät für Bauingenieurwesen, Technische Universität Wien; 2012, https://repositum.tuwien.at/handle/20.500.12708/13320.

[9] Dorn Michael, Habrová Karolína, Koubek Radek, Serrano Erik. Determination of coefficients of friction for laminated veneer lumber on steel under high pressure loads. Frict 2021;9(2):367–79. http://dx.doi.org/10.1007/S40544-020-0377-0.

[10] Aurand Simon, Blass Hans Joachim. Verbinder Aus Kunstharzpressholz Mit Erhöhter Reibung in der Scherfuge. In: Karlsruher Berichte Zum Ingenieurholzbau, vol. 38, Karlsruhe: KIT Scientific Publishing; 2023, http://dx.doi.org/10.5445/KSP/1000145949.

[11] Tomasi Roberto, Crosatti Alessandro, Piazza Maurizio. Theoretical and experimental analysis of timber-to-timber joints connected with inclined screws. Constr Build Mater 2010;24(9):1560–71. http://dx.doi.org/10.1016/J.Conbuildmat.2010.03.007.

[12] Jockwer Robert, Steiger René, Frangi Andrea. Design model for inclined screws under varying load to grain angles. In: Proceedings of INTER - meeting 47. Bath, United Kingdom; 2014, paper 47-7-5.

[13] Santis Yuri De, Fragiacomo Massimo. Timber-to-timber and steel-to-timber screw connections: Derivation of the slip modulus via beam on elastic foundation model. Eng Struct 2021;244. http://dx.doi.org/10.1016/J.Engstruct.2021.112798.

[14] Vella Nathan, Gardner Leroy, Buhagiar Spiridione. Analytical modelling of cold-formed steel-to-timber connections with inclined screws. Eng Struct 2021;249. http://dx.doi.org/10.1016/J.Engstruct.2021.113187.

[15] Caprio Dorotea, Jockwer Robert. Experimental investigation and probabilistic modelling of the load–displacement behaviour of steel-to-timber joints with self-tapping screws. Constr Build Mater 2025;489. http://dx.doi.org/10.1016/j.conbuildmat.2025.141970.

[16] Blass Hans Joachim, Steige Yvonne. Steifigkeit axial beanspruchter Vollgewindeschrauben. In: Karlsruher Berichte zum Ingenieurholzbau, vol. 34, Karlsruhe: KIT Scientific Publishing; 2018, http://dx.doi.org/10.5445/KSP/1000085040.

[17] Ehlbeck Jürgen, Freiseis Reinhold, Hättich Ronnie. Entwicklung und Prüfung neuer Verbindungsmittel aus Hartholz, Presschichtholz und ähnlichen holzhaltigen Werkstoffen für tragende Verbindungen im Holzbau. 1. Abschnitt: Mechanische und physikalische Eigenschaften von ausgewählten holzhaltigen Werkstoffen. Karlsruhe: Versuchsanstalt für Stahl, Holz und Steine, Abteilung für Ingenieurholzbau, Universität Karlsruhe(TH); 1985, http://dx.doi.org/10.5445/IR/1000173248.

[18] Ehlbeck Jürgen, Eberhart Otto. Entwicklung und Prüfung neuer Verbindungsmittel aus Hartholz, Presschichtholz und ähnlichen holzhaltigen Werkstoffen für tragende Verbindungen im Holzbau. Teil 2: Tragfähigkeits- und Verformungsverhalten von Verbindungen. A: Brettschichtholzverbindungen mit Stabdübeln aus Kunstharzpreßholz. Karlsruhe: Versuchsanstalt für Stahl, Holz und Steine, Abteilung für Ingenieurholzbau, Universität Karlsruhe(TH); 1989, http://dx.doi.org/10.5445/IR/1000173266.

[19] Ehlbeck Jürgen, Eberhart Otto. Entwicklung und Prüfung neuer Verbindungsmittel aus Hartholz, Presschichtholz und ähnlichen holzhaltigen Werkstoffen für tragende Verbindungen im Holzbau. Teil 2: Tragfähigkeits- und Verformungsverhalten von Verbindungen. B: Kerbuntersuchungen an Platten aus Kunstharzpreßholz. Karlsruhe: Versuchsanstalt für Stahl, Holz und Steine, Abteilung für Ingenieurholzbau, Universität Karlsruhe(TH); 1989, http://dx.doi.org/10.5445/IR/1000173268.

[20] Paulitsch Michael, Barbu Marius C. Holzwerkstoffe der Moderne. 1st ed. DRW-Verlag, Leinfelden-Echterdingen; 2015.

[21] Wagenführ André, Scholz Frieder. Taschenbuch der Holztechnik. 3rd ed. München: Carl Hanser Verlag; 2018, http://dx.doi.org/10.3139/9783446454415.

[22] Research Centre for Steel, Timber and Masonry. Test report no. 186147 (unpublished). 2018, KIT Timber Structures and Building Construction, Karlsruhe.

[23] Aurand Simon. A contribution to friction in timber connections. [Ph. D. thesis], Karlsruher Berichte zum Ingenieurholzbau, vol. 40, Karlsruhe: KIT Scientific Publishing; 2025, http://dx.doi.org/10.5445/KSP/1000176783.

[24] ETA-15/0187. Pitzl HVP connectors. 2023, ETA-Danmark A/S.
[25] ETA-19/0553. HECO-TOPIX-plus (or HTP or HT-plus), HECO-TOPIX-plus-T (or HTP-T or HT-plus-T) and HECO-TOPIX-plus-CC screws (or HTP-CC or HT-plus-CC) Screws for use in timber constructions. 2021, ETA-Danmark A/S.
[26] ETA-11/0190. Würth self-tapping screws. Berlin: Deutsches Institut für Bautechnik (DIBt); 2018, Deutsches Institut für Bautechnik.
[27] EN 26891. Timber structures; Joints made with mechanical fasteners; General principles for the determination of strength and deformation characteristic (ISO 6891:1983). 1991, CEN, Brussels.
[28] van de Kuilen Jan-Willem. Duration of load effects in timber joints. [Ph.D. thesis], Delft, The Netherlands: Delft University of Technology; 1999.
[29] Gräfe Martin. Vorgespannte Konstruktionen aus Brettsperrholz – Entwicklung, experimentelle und theoretische Untersuchungen, Entwurf und Bemessung. [Ph. D. thesis], München: Technische Universität München, Ingenieurfakultät Bau Geo Umwelt; 2020.
[30] EN 755-2. Aluminium and aluminium alloys – Extruded rod/bar, tube and profiles – Part 2: Mechanical properties. 2025, CEN, Brussels.
[31] Blaß Hans Joachim, Bejtka Ireneusz, Uibel Thomas. Tragfähigkeit von Verbindungen mit selbstbohrenden Holzschrauben mit Vollgewinde. Karlsruher Berichte zum Ingenieurholzbau, vol. 4. Karlsruhe: Universitätsverlag Karlsruhe; 2006, http://dx.doi.org/10.5445/KSP/1000004810.
[32] FprEN 1995-1-1:2025-04. Eurocode 5: Design of timber structures - Part 1–1. 2025, General rules and rules for buildings, CEN, Brussels.
[33] EN 1995-1-1:2010-12. Eurocode 5: Design of timber structures – Part 1–1. 2012, General – Common rules and rules for buildings, CEN, Brussels.
[34] Kevarinmäki Ari. Joints with inclined screws. In: Proceedings of CIB W18 - meeting 35. Kyoto, Japan; 2002, paper 35-7-3.
[35] Bejtka Ireneusz. Verstärkung von Bauteilen aus Holz mit Vollgewindeschrauben. [Ph. D. thesis], Karlsruher Berichte zum Ingenieurholzbau, vol. 2, Karlsruhe: Universitätsverlag Karlsruhe; 2005, http://dx.doi.org/10.5445/KSP/1000003354.
[36] Günter Steck. Die Zuverlässigkeit des Vollholzbalkens unter reiner Biegung. [Ph. D. thesis], Universität Karlsruhe; 1982, http://dx.doi.org/10.5445/IR/1000173271, Fakultät für Bauingenieur- und Vermessungswesen.
[37] Blass Hans Joachim. Moment-Normalkraft-Querkraft Interaktion in stiftförmigen Verbindungsmitteln von Stahlblech-Holz-Verbindungen. 2018, http://dx.doi.org/10.5445/IR/1000086376, Karlsruher Tage 2018 Holzbau, Karlsruhe.
[38] van de Kuilen Jan-Willem, Dias Alfredo. Creep factors for timber-timber and timber-concrete joints. In: Studies and researches, vol. 34, Milan, Italy: Graduate School in Concrete Structures – Fratelli Pesenti, Politecnico di Milano; 2015.
[39] EN 14358:2016-11. Timber structures – Calculation and verification of characteristic values; German version. 2016.